

Small-World Disordered Lattices: Spectral Gaps and Diffusive Transport

Matheus I. N. Rosa¹ and Massimo Ruzzene¹

¹*Department of Mechanical Engineering,
University of Colorado Boulder, Boulder CO 80309**

(Dated: March 31, 2022)

arXiv:2203.10381v2 [physics.app-ph] 29 Mar 2022

Abstract

We investigate the dynamic behavior of lattices with disorder introduced through non-local network connections. Inspired by the Watts-Strogatz small-world model, we employ a single parameter to determine the probability of local connections being re-wired, and to induce transitions between regular and disordered lattices. These connections are added as non-local springs to underlying periodic one-dimensional (1D) and two-dimensional (2D) square, triangular and hexagonal lattices. Eigenmode computations illustrate the emergence of spectral gaps in various representative lattices for increasing degrees of disorder. These gaps manifest themselves as frequency ranges where the modal density goes to zero, or that are populated only by localized modes. In both cases, we observe low transmission levels of vibrations across the lattice. Overall, we find that these gaps are more pronounced for lattice topologies with lower connectivity, such as the 1D lattice or the 2D hexagonal lattice. We then illustrate that the disordered lattices undergo transitions from ballistic to super-diffusive or diffusive transport for increasing levels of disorder. These properties, illustrated through numerical simulations, unveil the potential for disorder in the form of non-local connections to enable additional functionalities for metamaterials. These include the occurrence of disorder-induced spectral gaps, which is relevant to frequency filtering devices, as well as the possibility to induce diffusive-type transport which does not occur in regular periodic materials, and that may find applications in dynamic stress mitigation.

I. INTRODUCTION

Complex networks describe a wide variety of systems in nature and society. In particular, the small-world network model proposed by Watts and Strogatz [1] allows the exploration of the space between regular and random networks. In this model, the vertices of a regular network are re-wired with a probability p to another randomly selected node. This leads to networks that simultaneously exhibit a high degree of clustering, which is characteristic of regular networks, and short vertex-to-vertex distances, which characterizes random networks. Apart from the general characterization of its properties, [2–6] the small-world model has been applied to a variety of scenarios such as in the dynamics of epidemic spreading, [7, 8] and for modeling of brain, [9, 10] social, [11] and transportation networks. [12, 13]

* matheus.rosa@colorado.edu, massimo.ruzzene@colorado.edu

The physics of condensed matter systems based on small-world networks has also been explored in the form of Ising models, [14], to explore the onset of localization [15, 16] along with transport in quantum lattices [17–19].

In this paper, we investigate the dynamics of simple elastic lattices where non-local connections are inspired by the small-world network model. In the context of phononics and elastic metamaterials, [20] the role of disorder has attracted considerable interest. For example, rainbow-based materials have been investigated for band gap widening and energy trapping [21–27], for wave localization [28], to study the occurrence of topological phase transitions [29] and for signal processing applications [30]. Also, the role of disorder has been explored in the context of phonon and thermal transport [31, 32], and as part of the exploration of quasi-periodic lattices. [33–41] So far, most of prior studies have considered disorder introduced to local parameters or couplings, and the introduction of disorder through non-local connections defined by a network model has not yet been explored. To this end, we consider regular mono-atomic spring-mass lattices in the form of 1D lattices and of 2D hexagonal, square and triangular topologies, where connections are added based on the small-world model characterized by a chosen level of disorder. We first investigate the emergence of spectral gaps as a function of disorder through eigenmode computations performed on large lattices, and for multiple disorder realizations. Robust gaps appear in the form of frequency regions not populated by any modes, or populated only by localized modes, both resulting in low transmission levels across the lattice. These gaps appear to be more pronounced for topologies of lower connectivity, i.e. 1D and 2D hexagonal lattices which exhibit larger gaps than square and triangular lattices. Also, the analysis of transient wave behavior allows the characterization of the transport properties and the identification of transitions from ballistic to super-diffusive and diffusive transport. These are similar to the transitions experienced by quantum and photonic lattices in the presence of on-site disorder [42, 43]. The investigations presented herein identify a new route for introducing disorder in metamaterials in the form of non-local connections, which holds potential for the generation of disorder-resilient spectral gaps and for applications related to impact mitigation that leverage diffusive transport, as opposed to ballistic spreading observed in periodic materials.

This paper is organized as follows: following this introduction, section II describes the modeling of the small-world phononic lattices and the associated equations of motion. Next,

section III describes the spectral properties of the lattices and the emergence of band gaps through the non-local disordered links. Section IV then describes the transport properties of the network lattices and characterizes the transition from ballistic to diffusive transport. Finally, section V summarizes the main findings of this work and outlines future research directions.

II. SMALL-WORLD PHONONIC LATTICES: DESCRIPTION AND EQUATIONS

Figure 1 illustrates the considered 1D lattices, which consist of equal masses m (in red) connected to nearest neighbors and to the ground by springs of stiffness k_0 . These connections form periodic lattices which are here considered as baselines. Additional connections through springs k_n , represented as blue lines, connect nodes according to the small-network model based on a probability $p \in [0, 1]$. The case of $p = 0$ defines additional nearest neighbor connections (Figs. 1(a,b)), while $p \in (0, 1]$ in general defines the probability of rewiring to randomly chosen nodes (Figs. 1(c,d)). The same approach is employed for the 2D lattices in Fig. 2, which shows examples of hexagonal, square and triangular lattices with $p = 0$ (a,b,c), and with $p = 0.2$ (d,e,f). The presence of an underlying lattice guarantees that all the masses are connected, which is not enforced by the small-world network (blue) alone for arbitrary values of p . [1] Also, we elect that the spring constants are inversely proportional to the distance, i.e $k_{n,s} = \alpha k_0 / d_{n,s}$, where $d_{n,s}$ denotes the distance separating masses indexed by n and s , while α defines indicates the strength of these connections compared to the underlying lattice. This choice is motivated by the desire to retain the physical behavior of couplings in a mechanical lattice, whereby stiffness terms are typically inversely proportional to the length of the connection.

The equation of motion for a mass of index n is expressed as:

$$m\ddot{u}_n + k_0 u_n + \sum_r k_0 (u_n - u_r) + \alpha \sum_s \frac{k_0}{d_{n,s}} (u_n - u_s) = f_n, \quad (1)$$

where r runs over the nearest neighbors, and s runs over the network links that connect to that mass, while u_n and f_n represent the displacement and the force applied to the n -th mass. For a finite lattice of N masses, the equations of motion can be assembled in matrix

form:

$$\mathbf{M}\ddot{\mathbf{u}} + \mathbf{K}\mathbf{u} = \mathbf{f}, \quad (2)$$

where $\mathbf{u} = [u_1, u_2, \dots, u_N]^T$, $\mathbf{f} = [f_1, f_2, \dots, f_N]^T$, and \mathbf{M}, \mathbf{K} respectively denote the mass and stiffness matrices. The numerical results presented in this paper rely on standard procedures such as numerical solution of the eigenvalue problem $\mathbf{K}\mathbf{u} = \omega^2\mathbf{M}\mathbf{u}$ for the natural frequencies and mode shapes of the lattice, and numerical integration of the equations of motion for evaluating the transient behavior under a set of initial conditions, both in the absence of external forcing. Additionally, we evaluate the lattice response for assigned harmonic forcing $\mathbf{f}(t) = \mathbf{f}_0 e^{i\omega t}$ by numerically solving the linear system $(-\omega^2\mathbf{M} + \mathbf{K})\mathbf{u} = \mathbf{f}_0$, with \mathbf{f}_0 being the vector of forcing amplitudes at frequency ω .

III. SPECTRAL PROPERTIES AND BAND GAP EMERGENCE

We first investigate the spectral properties of the network lattices and the emergence of band gaps. Due to the absence of periodicity, we rely on eigen-mode computations performed on representative finite lattices. Figure 3(a) illustrates an example for a finite lattice with

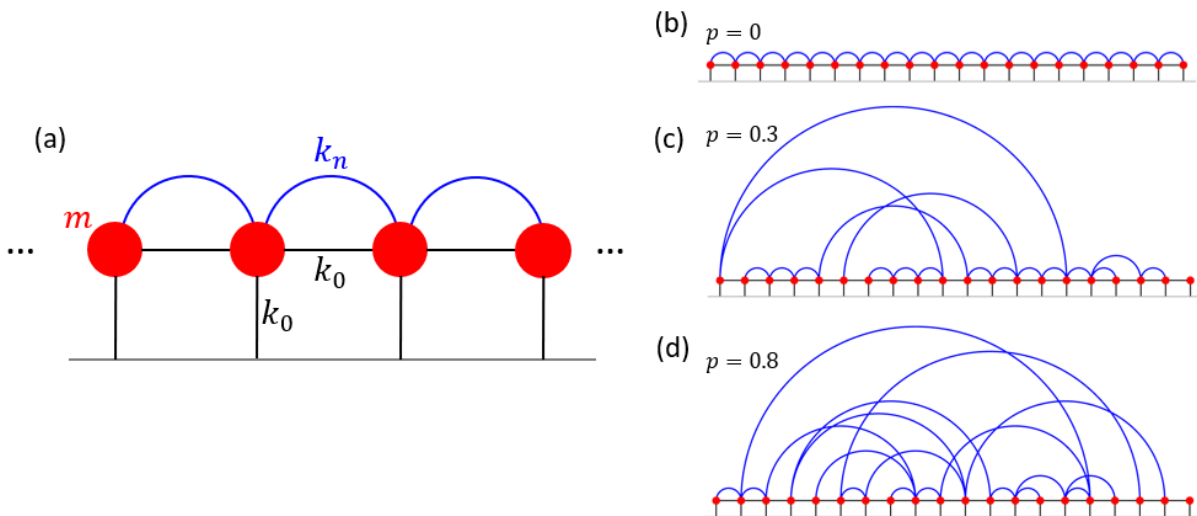


FIG. 1. Schematics of 1D small-world network lattices. Each mass (red) is connected to the nearest neighbors and to the ground by a spring of constant k_0 (black lines) (a). Additional network connections are represented by blue links, which initially also connect nearest neighbors and are re-wired with probability p to another random node. Examples with $N = 20$ masses and $p = 0, 0.3, 0.8$ are illustrated in (b,c,d).

$N = 50$ masses and $\alpha = 5$, and compares the eigen-frequencies computed for two lattices with $p = 0$ and $p = 0.6$ under free-free boundary conditions. Throughout this paper, we employ $\Omega = \omega/\omega_0$ as a normalized frequency, where $\omega_0 = \sqrt{k_0/m}$. The dots corresponding to each frequency value are color-coded based on the Inverse Participation Ratio (IPR) of

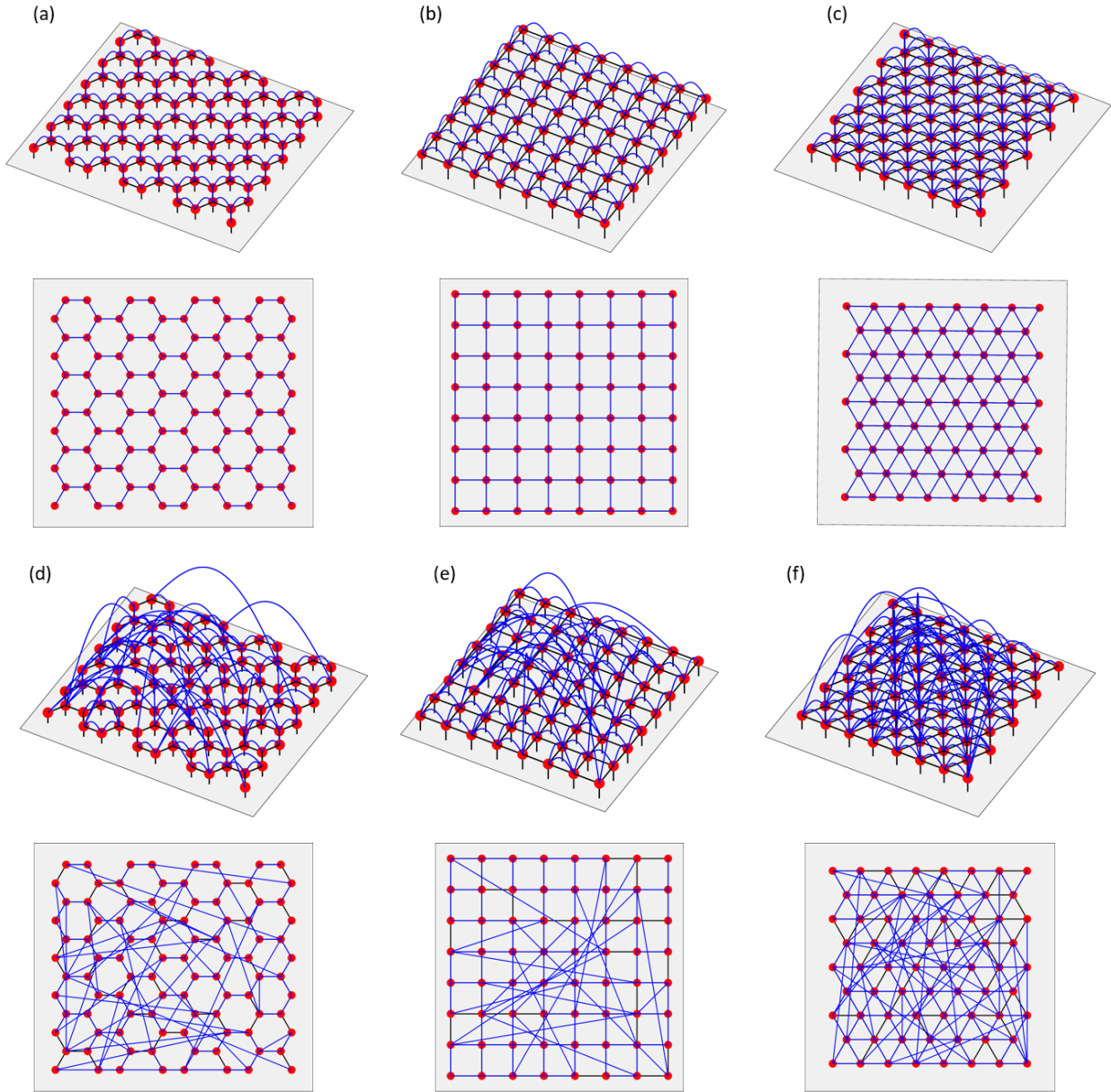


FIG. 2. Two-dimensional hexagonal, square and triangular small-world network lattices with $p = 0$ (a,b,c) and $p = 0.2$ (d,e,f). The top and bottom rows respectively display the perspective and top views, with network links represented by blue lines.

the corresponding modes, which is defined as:

$$IPR = \frac{\sum_n |u_n|^4}{(\sum_n |u_n|^2)^2}, \quad (3)$$

where u_n is the n_{th} component of the eigenvector. The IPR varies from 0 to 1 and signals whether a mode is localized or not when its value is high or low, respectively. A few modes are marked in Fig. 3(a) and have their mode shapes displayed in Fig. 3(b). When $p = 0$, the frequencies of the lattice define a continuous band with only non-localized modes, as expected of a periodic monoatomic lattice [20]. However, the lattice with $p = 0.6$ supports a series of localized modes, with two examples displayed in Fig. 3(b). While localized modes are expected to appear due to the presence of disorder, we also note that a few frequency bands are not populated by any modes and may potentially define band gaps. Naturally, these results correspond to a single realization of the lattice, and are not sufficient to draw conclusions about the behavior expected of any realization due to the randomness of the non-local connections.

To obtain further insight into the spectral properties of the network lattices, we compute the modes of a large finite lattice comprising $N = 500$ masses for p varying from 0 to 1, for multiple realizations and for multiple values of α , with results summarized in Fig. 4(a). Each column corresponds to one α value ranging from 1 to 5: the top row displays the frequencies

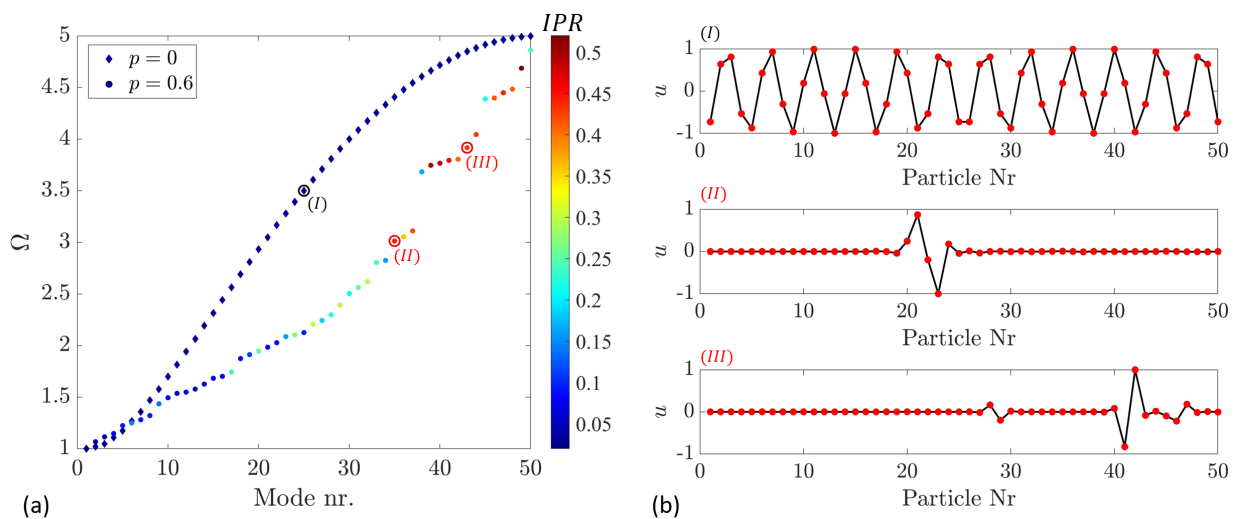


FIG. 3. Eigenfrequencies (a) and selected mode shapes (b) of finite lattice with $N = 50$ masses and free-free boundary conditions for $p = 0$ and $p = 0.6$. The frequencies in (a) are color-coded according to their IPR, signaling whether the modes are localized or not.

as a function of p for a single lattice realization, while the bottom row superimposes the frequencies of 100 different random realizations of each p value. In both cases, the color is associated with the IPR. The results confirm the existence of frequency bands where no modes exist, which emerge for increasing values of p , and are more pronounced for larger values of α . The presence of these spectral gaps is further confirmed by evaluating the harmonic response of a lattice with $N = 200$ masses, excited by a harmonic force at the center mass. The harmonic response is computed as described in section II, and we define the transmission as the \mathcal{L}_2 norm of the response along the lattice divided by the response at the input site n_0 , i.e. $T = \|\mathbf{u}/u_{n_0}\|_2$. The transmission is averaged across 100 realizations for varying p and Ω , and is displayed as log-scale colormaps in Fig. 4(b) for the different α values. We note that for $\alpha = 1$ a few gaps appear for a single realization, which are mostly filled by localized modes characterized by a high IPR when multiple realizations are considered. For $\alpha = 3$ and $\alpha = 5$, some gaps are persistent without any existing modes even for multiple realizations, signaling a degree of robustness. The transmission results in Fig. 4(b) confirm the existence of the spectral gaps that are not occupied by any modes, and also of the gaps that are populated by a high density of localized modes. Indeed, localized modes are not associated with transport along the lattice, and therefore are associated with frequency regions of low vibration transmission along the length of the lattice. These results illustrate that the addition of small-world networks of springs of sufficient strength produce well defined spectral gaps that emerge due to the disordered network connections, and persist across multiple lattice realizations. We also note the presence of thin bands of high transmission at fixed frequencies spanning large p intervals, for example at $\Omega = 2.5, 3.4$ with $\alpha = 3$, and $\Omega = 2.8, 4.2$ with $\alpha = 5$, which signal another robust feature emanating from such disordered lattices.

Next, we investigate the spectral properties of 2D lattices. Results for $\alpha = 5$ are summarized in Fig. 5, which displays the frequencies of 61×61 lattices as a function of p . As in previous figures, the spectral properties are color-coded in terms of the IPR, and are obtained considering 100 different realizations of hexagonal (a), square (b) and triangular (c) lattices. The bottom panels (d,e,f) display the transmission as a function of p and Ω , which are obtained for 41×41 lattices excited at the center mass and by averaging the response of 100 lattice realizations. While no regions that are not populated by any modes are found, there is evidence of regions populated only by localized modes emerging with increasing

p . As in the 1D case, these regions filled by localized modes correspond to regions of low transmission, as confirmed by the plots in (d,e,f). In the hexagonal case, a couple of regions within the spectrum filled with localized modes are observed to emerge in Fig. 5(a), which are confirmed by low transmission regions in (d). The size of the gaps within the spectrum are diminished in the square lattice case (b,e), and become very small in the triangular lattice case (c,f). These results illustrate how the lattice topology plays an important role in the emergence of bandgaps, and suggest that the progressive increase in connectivity from the 1D lattice (2 connections per node) to the triangular lattice (6 connections per node) causes a decrease in band gap occurrence. In particular to the 2D case, we note that low frequency gaps seem to emerge as a function of p as the first mode of the lattice is separated by a gap from the collective of the other modes of the lattice. The width of this gap increases with the lattice connectivity, i.e. it appears wider in triangular lattices than in the hexagonal ones. Although the spectral properties of these lattices are largely influenced by the topology, in the next section we illustrate that the transport properties are qualitatively similar and that transitions to diffusive transport can be observed in all cases.

IV. TRANSIENT BEHAVIOR: FROM BALLISTIC TO DIFFUSIVE TRANSPORT

The transient behavior of the small-world lattices is investigated next. We characterized wave motion in disordered lattices by relying on a approach [43, 44] that considers the dynamic evolution of the lattice motion resulting from an initial perturbation. Such evolution is quantified by computing the Mean Square Displacement (MSD), which is defined as

$$MSD(t) = \left\langle \sum_n (d_{n,n_0})^2 |u_n(t)|^2 \right\rangle \approx t^\gamma, \quad (4)$$

Here, $\langle \rangle$ denotes the averaging operation across multiple lattice realizations, n_0 is the site where the initial perturbation is applied, and d_{n,n_0} is the distance between the generic site n and n_0 . The MSD is found to scale as t^γ , where t denotes time while the exponent γ quantifies the rate of perturbation spreading. Thus, γ is used to classify the type of transport that occurs along the medium. For example, quantum and photonic periodic lattices, which are governed by similar equations of motion, exhibit *ballistic* transport which is characterized

by $\gamma = 2$ [43, 44]. In the presence of disorder, decreasing values of γ quantify the slower spread that occurs in comparison to regular periodic materials. For instance, depending on the amount of disorder, lattices may exhibit super-diffusive ($\gamma = 1.5$) or diffusive ($\gamma = 1$) transport, or absence of transport altogether for $\gamma \approx 0$, which corresponds to the onset of Anderson Localization [42, 43, 45]. This approach has been recently applied to other types of aperiodic systems, for example in fractal lattices where γ is found to be related to

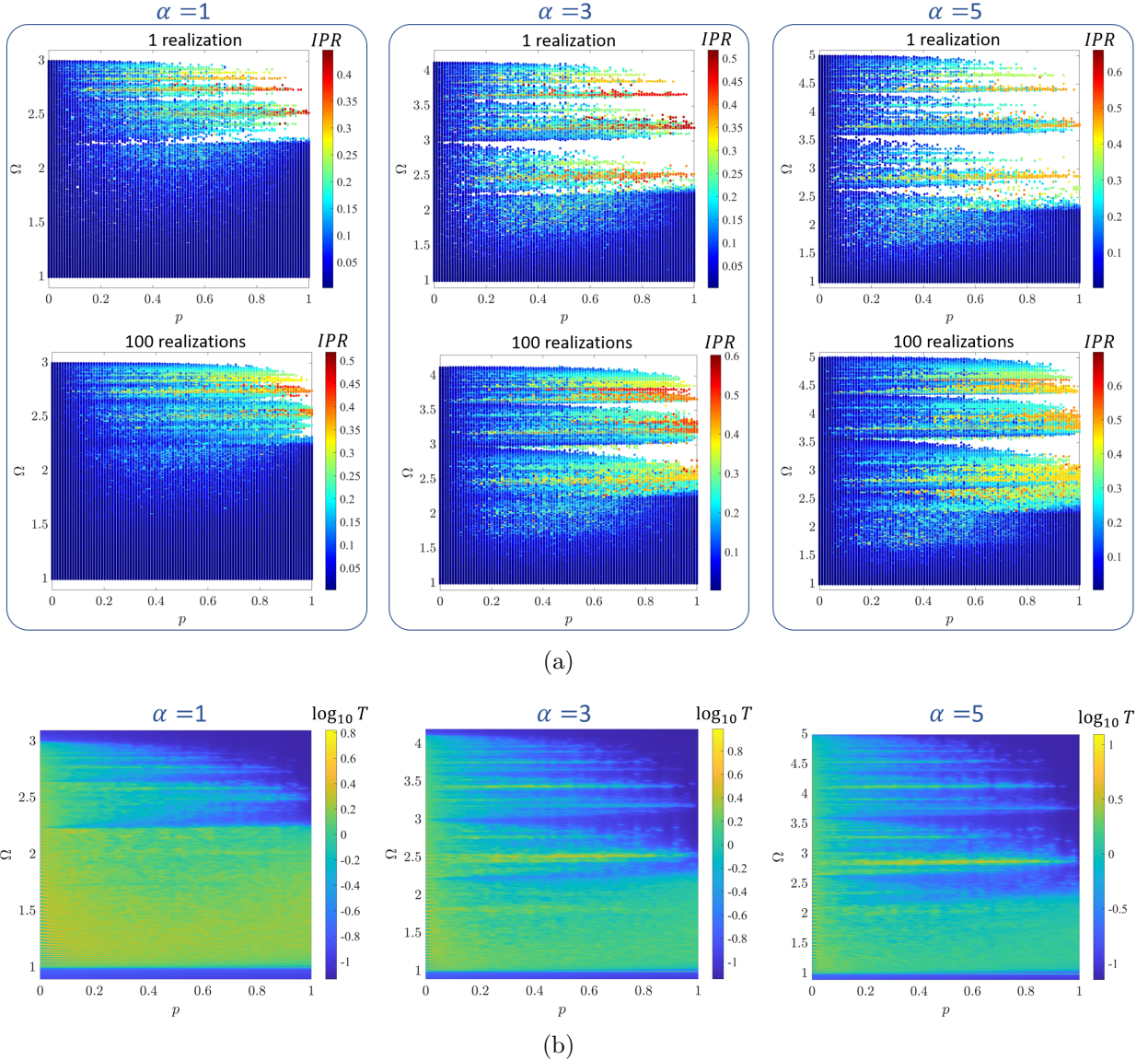


FIG. 4. Spectral properties of 1D small-world phononic lattices. Eigenfrequencies of finite lattice with $N = 500$ masses computed as a function of p for multiple α values and 1 (top) or 100 (bottom) lattice realizations, color coded by the IPR (a). Transmission of finite lattice with $N = 200$ masses when excited at the center as a function of p , averaged along the lattice and across 100 realizations, for multiple α values (b).

the fractal dimension of the lattice, [46] and also for the characterization of wave packets spreading in disordered non-linear architected materials [47].

Here, we adopt the MSD to characterize the transport in the small-world lattices. Starting from the 1D case, we consider a large lattice with $N = 1000$ masses and apply a perturbation to the $n_0 = 500$ site. The perturbation is in the form of initial conditions $u_{n_0}(0) = 0, \dot{u}_{n_0}(0) = 1$, which are equivalent to an impulse excitation $f(t) = \delta(t)$ applied to the chosen site. This excitation involves the entire spectrum of the lattice and is similar to the excitation applied to photonic lattices at $z = 0$, where z is the propagation dimension [43]. We observe the spreading for a series of 1D lattices of different α values and evaluate its variation in terms of the disorder parameter p . The simulation time window is adjusted for each α based on the $p = 0$ case in order to avoid the presence of reflections at the boundaries, which would affect the MSD computations. For each α, p combination, the MSD is computed by averaging across 200 lattice realizations, and the resulting γ is extracted by fitting the tail of the corresponding $MSD(t)$ curve in logarithmic scale.

The results for the 1D lattices are summarized in Fig. 6. Figures 6(a,b) display the

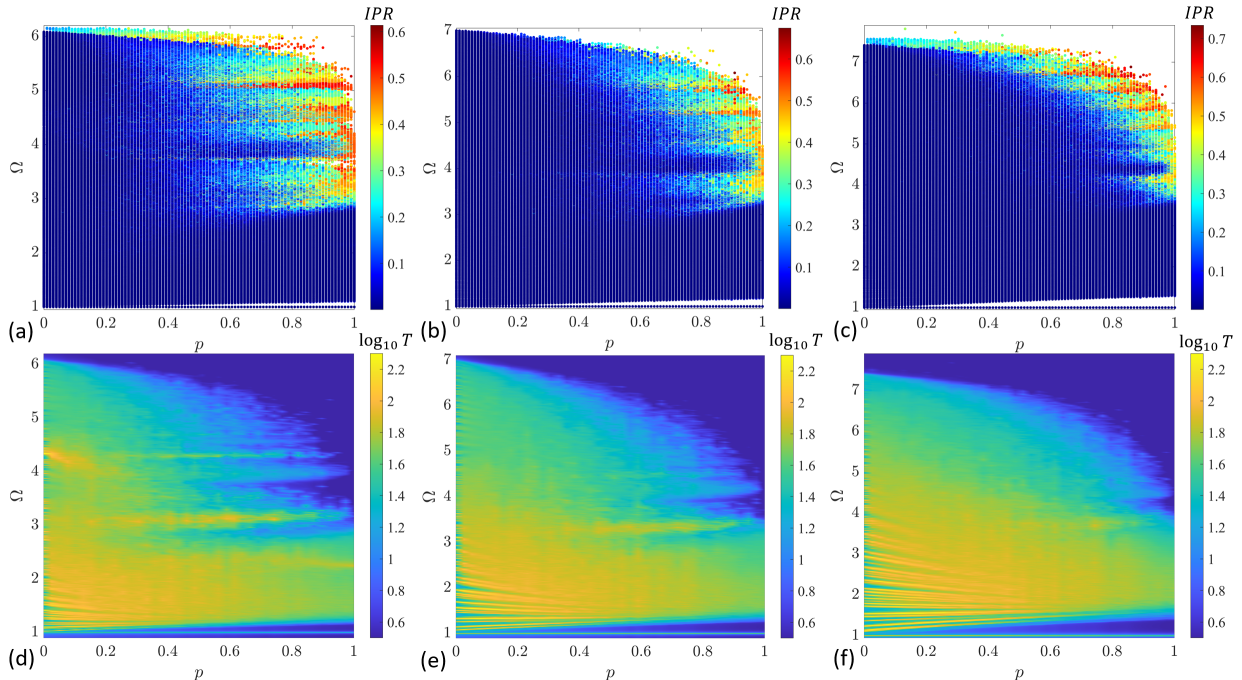


FIG. 5. Spectral properties of 2D network lattices. Top panels (a,b,c) display the eigenfrequencies of 61×61 hexagonal, square and triangular lattices, considering 100 realizations, and color-coded according to the IPR. The bottom panels (d,e,f) display the transmission averaged over 100 realizations for 41×41 hexagonal, square and triangular lattices.

average displacement field in absolute value for $\alpha = 0.5$ and $\alpha = 2.5$, and for increasing values of p . The results illustrate a decrease in the spreading of the perturbation caused by the increase in disorder from the baseline $p = 0$ case (left panels), as p increases to $p = 0.025$ (middle panels), and up to $p = 0.51$ (right panels). The quantification of the spreading using the MSD is illustrated in Figs. 6(c,d) by the plots in log scale. The circles superimposed to the tail of the MSD curves correspond to the numerically fitted relationship t^γ , allowing for the extraction of γ that quantifies the observed decrease in slope associated with the decrease in spreading. The exemplified procedure is repeated for multiple lattices resulting in Fig. 6(e), where the extracted γ values are directly plotted as a function of p for multiple α values ranging from 0.5 to 7.5. The figure provides a characterization of the transport properties of the lattice, illustrating that multiple transport regimes such as ballistic, super-diffusive and diffusive are achieved by different parameters p, α . In particular, we confirm that for $p = 0$, ballistic spreading characterized by $\gamma = 2$ occurs regardless of the α value, as expected from periodic lattices. As p increases, γ decreases along different transitions that are intensified for higher values of α . The results in Figs. 6(a,b) correspond to the points marked in Fig. 6(e), chosen to illustrate two transitions types. The one in Fig. 6(a) corresponds to a transition from ballistic to super-diffusive transport as γ approaches 1.5 for increasing disorder levels. The second example in Fig. 6(b) illustrates the transition from ballistic to diffusive transport as γ becomes closer to 1.

Next, the transport behavior for the 2D hexagonal, square and triangular lattices is illustrated in Fig. 7. The procedure for the 1D case is extended to 2D lattices of sizes 29×52 , 41×41 and 49×57 , respectively. The number of cells has been chosen in order to form domains of similar length along the x and y directions, and which are sufficiently large to observe the spreading of the perturbation applied as initial conditions to the center mass. Similar to the 1D case, the results are obtained upon averaging again over 200 realizations and extracting γ from the MSD curves for each p, α combination. Figures 7(a,b,c) display the resulting variation of γ with respect to p for the hexagonal, square and triangular lattices, with α ranging from 0.5 to 6. As in the 1D case, we again find that periodic lattices for $p = 0$ are characterized by ballistic transport properties associated with $\gamma = 2$. This is verified for any value of α for all the lattice topologies considered, and it is expected for periodic lattices in general. [44] The figures also illustrate how multiple transport regimes are achieved in all lattice topologies by different choices of p, α . Two transitions with $\alpha = 2$

and $\alpha = 6$ are exemplified for the hexagonal lattice, where the points marked in Fig. 7(a) have their corresponding averaged displacement fields displayed in panels (d,e). The plots show the absolute value of displacement across the lattice in the x, y plane at 5 subsequent time instants, with time varying along the vertical axis. The displacement for a sectional x, t plane defined for the center y coordinate is also plotted to improve the visualization of the wave spreading as a function of time. Also, due to the amplitude decrease resulting from wave spreading, the color axis in each plot is restricted to a range corresponding to 10% of the maximum displacement value along the entire time history. For $\alpha = 2$, a transition to super-diffusive behavior ($\gamma \approx 1.5$) is observed, while $\alpha = 6$ produces a transition to diffusive transport ($\gamma \approx 1$). The associated decrease in the spreading can be clearly observed in the displacement plots by observing how the wave front propagates shorter distances in the $p = 1$ cases when compared to the ballistic $p = 0$ cases. Overall, the transport transitions are very similar for all the considered 2D lattice topologies, with small qualitative differences in the γ variations with p and α .

These results illustrate how the disorder introduced through the network connections modify the type of transport for all the considered lattice topologies, causing a transition to super-diffusive or diffusive transport when the strength of the network connections (α) is sufficiently strong. These transitions are reminiscent of those experienced by quantum and photonic lattices with on-site disorder [42, 43]. However, we note that for the considered range of α values, γ reaches a plateau close to 1, and Anderson Localization ($\gamma \approx 0$) does not occur. Higher values $\alpha > 7.5$ are not considered herein since the network connections become much stronger and overcome the couplings of the underlying lattice. Our preliminary investigations showed that the transport in that case was not well captured by the MSD computations, similarly to findings in quantum lattices with distance-independent coupling and absence of an underlying lattice [17]. Such high α regime may be further investigated in the future.

V. CONCLUSIONS

In this paper, we investigate the dynamics of phononic lattices with small-world network connections. Our results illustrate the emergence of spectral gaps due to increasing degrees of disorder, which are persistent across multiple lattice realizations. Lattices of different

topologies, such as 1D and 2D hexagonal, square and triangular lattices were shown to feature transitions from ballistic to super-diffusive or diffusive transport. These results motivate a new route for the introduction of disorder in metamaterials through network connections, potentially leading to novel functionalities enabled by disorder such as spectral gaps and diffusive transport, which could be exploited in impact mitigation applications for example. The initial investigations presented here may be expanded in multiple directions in future studies. For example, a variety of other network modeling strategies may be

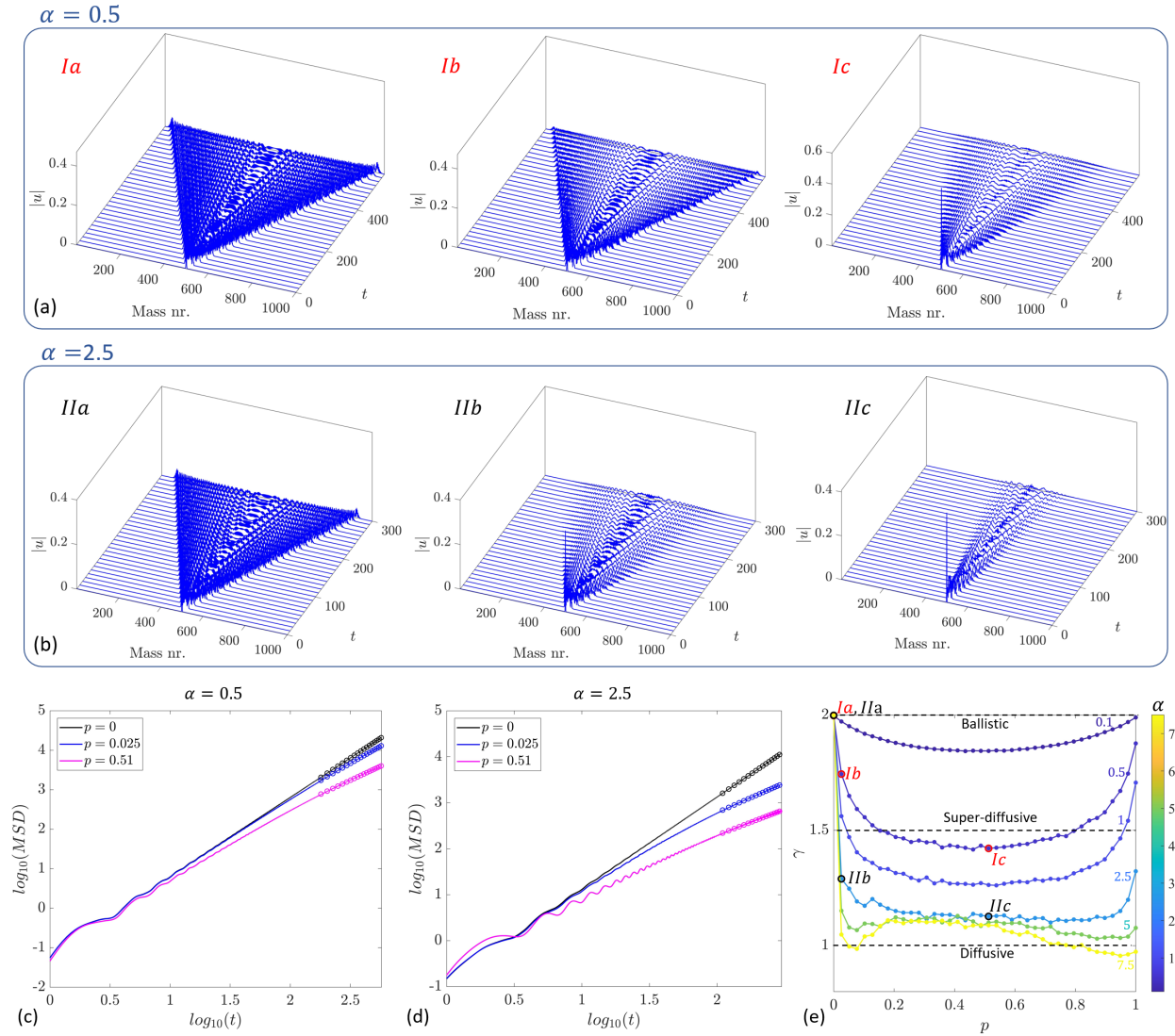


FIG. 6. Transport properties of 1D small-world network lattices. Average displacement fields for $\alpha = 0.5$ (a) and $\alpha = 2.5$ (b), with $p = 0$ (left), $p = 0.025$ (middle) and $p = 0.51$ (right). The fitting of the corresponding MSD curves is displayed in (c,d), with circles superimposed to the curves corresponding to fitted data. Variation of γ with p for multiple α values (e), with guidelines for ballistic, super-diffusive and diffusive transport.

considered, along with different underlying lattice topologies, different statistical modeling of non-local connections instead of random re-wiring, the introduction of non-linearities, as well as the experimental investigations of the transport properties, among others.

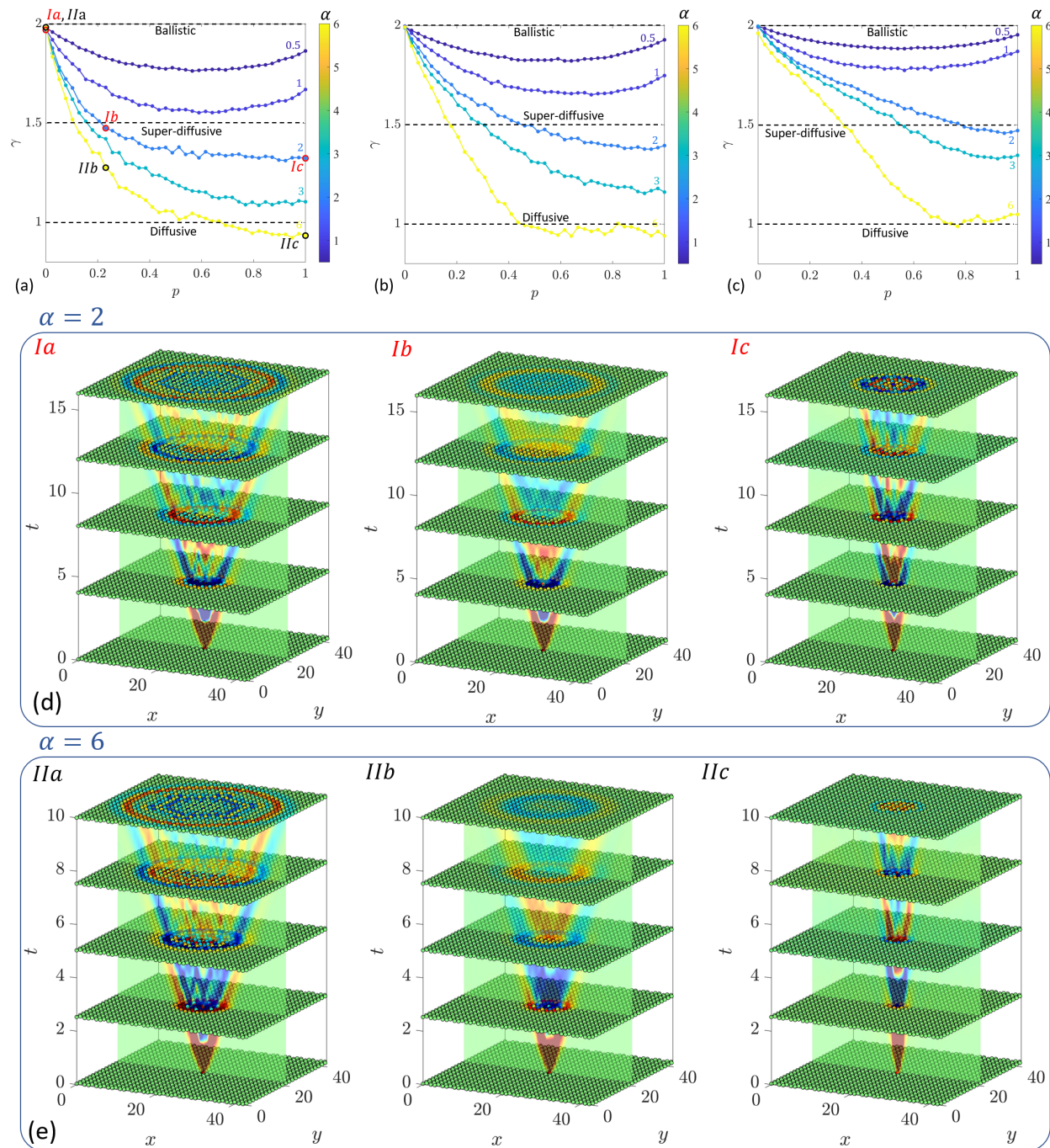


FIG. 7. Transport properties of 2D small-world network lattices. Variation of γ with p for hexagonal (a), square (b) and triangular (c) lattices, and for multiple α values ranging from 0.5 to 6. Examples marked in (a) have their corresponding averaged displacements displayed in (d,e).

ACKNOWLEDGMENTS

The authors gratefully acknowledge the support from the National Science Foundation (NSF) through the EFRI 1741685 grant and from the Army Research office through grant W911NF-18-1-0036.

- [1] Duncan J Watts and Steven H Strogatz. Collective dynamics of ‘small-world’ networks. *nature*, 393(6684):440–442, 1998.
- [2] Cristopher Moore and Mark EJ Newman. Exact solution of site and bond percolation on small-world networks. *Physical Review E*, 62(5):7059, 2000.
- [3] Alain Barrat and Martin Weigt. On the properties of small-world network models. *The European Physical Journal B-Condensed Matter and Complex Systems*, 13(3):547–560, 2000.
- [4] Mark EJ Newman. Models of the small world. *Journal of Statistical Physics*, 101(3):819–841, 2000.
- [5] Marc Barthélemy and Luis A Nunes Amaral. Small-world networks: Evidence for a crossover picture. In *The Structure and Dynamics of Networks*, pages 304–307. Princeton University Press, 2011.
- [6] Mark EJ Newman, DJ Walls, Mark Newman, Albert-László Barabási, and Duncan J Watts. Scaling and percolation in the small-world network model. In *The Structure and Dynamics of Networks*, pages 310–320. Princeton University Press, 2011.
- [7] Cristopher Moore and Mark EJ Newman. Epidemics and percolation in small-world networks. *Physical Review E*, 61(5):5678, 2000.
- [8] Mark EJ Newman, I Jensen, and RM Ziff. Percolation and epidemics in a two-dimensional small world. *Physical Review E*, 65(2):021904, 2002.
- [9] Danielle Smith Bassett and ED Bullmore. Small-world brain networks. *The neuroscientist*, 12(6):512–523, 2006.
- [10] Xuhong Liao, Athanasios V Vasilakos, and Yong He. Small-world human brain networks: perspectives and challenges. *Neuroscience & Biobehavioral Reviews*, 77:286–300, 2017.
- [11] Dan Braha and Yaneer Bar-Yam. The statistical mechanics of complex product development: Empirical and analytical results. *Management Science*, 53(7):1127–1145, 2007.

- [12] Vito Latora and Massimo Marchiori. Is the boston subway a small-world network? *Physica A: Statistical Mechanics and its Applications*, 314(1-4):109–113, 2002.
- [13] Michele Guida and Funaro Maria. Topology of the italian airport network: A scale-free small-world network with a fractal structure? *Chaos, Solitons & Fractals*, 31(3):527–536, 2007.
- [14] Carlos P Herrero. Ising model in small-world networks. *Physical Review E*, 65(6):066110, 2002.
- [15] Remi Monasson. Diffusion, localization and dispersion relations on “small-world” lattices. *The European Physical Journal B-Condensed Matter and Complex Systems*, 12(4):555–567, 1999.
- [16] Chen-Ping Zhu and Shi-Jie Xiong. Localization-delocalization transition of electron states in a disordered quantum small-world network. *Physical Review B*, 62(22):14780, 2000.
- [17] Beom Jun Kim, H Hong, and MY Choi. Quantum and classical diffusion on small-world networks. *Physical Review B*, 68(1):014304, 2003.
- [18] Oliver Mülken, Volker Pernice, and Alexander Blumen. Quantum transport on small-world networks: A continuous-time quantum walk approach. *Physical Review E*, 76(5):051125, 2007.
- [19] S Çalışkan, MA Novotny, and Jorge I Cerdá. Transport through small world networks. *Journal of applied physics*, 102(1):013707, 2007.
- [20] Mahmoud I Hussein, Michael J Leamy, and Massimo Ruzzene. Dynamics of phononic materials and structures: Historical origins, recent progress, and future outlook. *Applied Mechanics Reviews*, 66(4):040802, 2014.
- [21] Jie Zhu, Yongyao Chen, Xuefeng Zhu, Francisco J Garcia-Vidal, Xiaobo Yin, Weili Zhang, and Xiang Zhang. Acoustic rainbow trapping. *Scientific reports*, 3(1):1–6, 2013.
- [22] Davide Cardella, Paolo Celli, and Stefano Gonella. Manipulating waves by distilling frequencies: a tunable shunt-enabled rainbow trap. *Smart Materials and Structures*, 25(8):085017, 2016.
- [23] Zhenhua Tian and Lingyu Yu. Rainbow trapping of ultrasonic guided waves in chirped phononic crystal plates. *Scientific reports*, 7(1):1–7, 2017.
- [24] Paolo Celli, Behrooz Yousefzadeh, Chiara Daraio, and Stefano Gonella. Bandgap widening by disorder in rainbow metamaterials. *Applied Physics Letters*, 114(9):091903, 2019.
- [25] Danilo Beli, Adriano T Fabro, Massimo Ruzzene, and José Roberto F Arruda. Wave attenuation and trapping in 3d printed cantilever-in-mass metamaterials with spatially correlated variability. *Scientific reports*, 9(1):1–11, 2019.

- [26] Jacopo M De Ponti, Andrea Colombi, Emanuele Riva, Raffaele Ardito, Francesco Braghin, Alberto Corigliano, and Richard V Craster. Experimental investigation of amplification, via a mechanical delay-line, in a rainbow-based metamaterial for energy harvesting. *Applied Physics Letters*, 117(14):143902, 2020.
- [27] Renan L Thomes, Jaime A Mosquera-Sánchez, and Carlos De Marqui Jr. Bandgap widening by optimized disorder in one-dimensional locally resonant piezoelectric metamaterials. *Journal of Sound and Vibration*, 512:116369, 2021.
- [28] J Flores, L Gutiérrez, RA Méndez-Sánchez, G Monsivais, Pierric Mora, and A Morales. Anderson localization in finite disordered vibrating rods. *EPL (Europhysics Letters)*, 101(6):67002, 2013.
- [29] Xiaotian Shi, Ioannis Kiorpelidis, Rajesh Chaunsali, Vassos Achilleos, Georgios Theocharis, and Jinkyu Yang. Disorder-induced topological phase transition in a one-dimensional mechanical system. *Physical Review Research*, 3(3):033012, 2021.
- [30] Farzad Zangeneh-Nejad and Romain Fleury. Disorder-induced signal filtering with topological metamaterials. *Advanced Materials*, 32(28):2001034, 2020.
- [31] Markus R Wagner, Bartłomiej Graczykowski, Juan Sebastian Reparaz, Alexandros El Sachat, Marianna Sledzinska, Francesc Alzina, and Clivia M Sotomayor Torres. Two-dimensional phononic crystals: Disorder matters. *Nano letters*, 16(9):5661–5668, 2016.
- [32] Shiqian Hu, Zhongwei Zhang, Pengfei Jiang, Weijun Ren, Cuiqian Yu, Junichiro Shiomi, and Jie Chen. Disorder limits the coherent phonon transport in two-dimensional phononic crystal structures. *Nanoscale*, 11(24):11839–11846, 2019.
- [33] David J Apigo, Kai Qian, Camelia Prodan, and Emil Prodan. Topological edge modes by smart patterning. *Physical Review Materials*, 2(12):124203, 2018.
- [34] Matheus IN Rosa, Raj Kumar Pal, José RF Arruda, and Massimo Ruzzene. Edge states and topological pumping in spatially modulated elastic lattices. *Physical review letters*, 123(3):034301, 2019.
- [35] David J Apigo, Wenting Cheng, Kyle F Dobiszewski, Emil Prodan, and Camelia Prodan. Observation of topological edge modes in a quasiperiodic acoustic waveguide. *Physical review letters*, 122(9):095501, 2019.
- [36] Xiang Ni, Kai Chen, Matthew Weiner, David J Apigo, Camelia Prodan, Andrea Alu, Emil Prodan, and Alexander B Khanikaev. Observation of hofstadter butterfly and topological edge

- states in reconfigurable quasi-periodic acoustic crystals. *Communications Physics*, 2(1):1–7, 2019.
- [37] Raj Kumar Pal, Matheus IN Rosa, and Massimo Ruzzene. Topological bands and localized vibration modes in quasiperiodic beams. *New Journal of Physics*, 21(9):093017, 2019.
- [38] Yiwei Xia, Alper Erturk, and Massimo Ruzzene. Topological edge states in quasiperiodic locally resonant metastructures. *Physical Review Applied*, 13(1):014023, 2020.
- [39] Mohit Gupta and Massimo Ruzzene. Dynamics of quasiperiodic beams. *Crystals*, 10(12):1144, 2020.
- [40] Matheus IN Rosa, Yuning Guo, and Massimo Ruzzene. Exploring topology of 1d quasiperiodic metastructures through modulated lego resonators. *Applied Physics Letters*, 118(13):131901, 2021.
- [41] Matheus IN Rosa, Massimo Ruzzene, and Emil Prodan. Topological gaps by twisting. *Communications Physics*, 4(1):1–10, 2021.
- [42] David H Dunlap, HL Wu, and Philip W Phillips. Absence of localization in a random-dimer model. *Physical Review Letters*, 65(1):88, 1990.
- [43] U Naether, S Stützer, RA Vicencio, MI Molina, A Tünnermann, S Nolte, Tsampikos Kottos, DN Christodoulides, and A Szameit. Experimental observation of superdiffusive transport in random dimer lattices. *New Journal of Physics*, 15(1):013045, 2013.
- [44] Hao Tang, Xiao-Feng Lin, Zhen Feng, Jing-Yuan Chen, Jun Gao, Ke Sun, Chao-Yue Wang, Peng-Cheng Lai, Xiao-Yun Xu, Yao Wang, et al. Experimental two-dimensional quantum walk on a photonic chip. *Science advances*, 4(5):eaat3174, 2018.
- [45] Philip W Anderson. Absence of diffusion in certain random lattices. *Physical review*, 109(5):1492, 1958.
- [46] Xiao-Yun Xu, Xiao-Wei Wang, Dan-Yang Chen, C Morais Smith, and Xian-Min Jin. Quantum transport in fractal networks. *Nature Photonics*, 15(9):703–710, 2021.
- [47] Arnold Ngapasare, Georgios Theocharis, Olivier Richoux, Vassos Achilleos, et al. Wave-packet spreading in disordered soft architected structures. *arXiv preprint arXiv:2203.00383*, 2022.